J. Fluid Mech. (1992), *vol.* 238, *pp.* 73–96
Printed in Great Britain

The flow over a backward-facing step under controlled perturbation: laminar separation

By M. A. Z. HASAN
Mechanical Engineering Department, King Fahd University of Petroleum & Minerals, Dhahran 31261, Saudi Arabia

(Received 15 August 1989 and in revised form 17 June 1991)

The flow over a backward-facing step with laminar separation was investigated experimentally under controlled perturbation for a Reynolds number of 11000, based on a step height h and a free-stream velocity U_0. The reattaching shear layer was found to have two distinct modes of instability: the 'shear layer mode' of instability at $St_\theta \approx 0.012$ ($St_\theta \equiv f\theta/U_0$, θ being the momentum thickness at separation and f the natural roll-up frequency of the shear layer); and the 'step mode' of instability at $St_h \approx 0.185$ ($St_h \equiv fh/U_0$). The shear layer instability frequency reduced to the step mode one via one or more stages of a vortex merging process. The perturbation increased the shear layer growth rate and the turbulence intensity and decreased the reattachment length compared to the unperturbed flow. Cross-stream measurements of the amplitudes of the perturbed frequency and its harmonics suggested the splitting of the shear layer. Flow visualization confirmed the shear layer splitting and showed the existence of a low-frequency flapping of the shear layer.

1. Introduction

Turbulent shear flows with separation and subsequent reattachment are grouped under complex flows. High turbulence intensity and localized mean or instantaneous reverse flow are common to these flows. Based on the flow geometry, such flows are usually classified into four groups (figure 1). Flows with separation and reattachment are fairly common in practical engineering devices, such as airfoils with a separation bubble, buildings, combustors, pipes with expansion, yet after four decades of research, our understanding of reattaching flows is far from complete.

The first review of the experimental data for reattaching flows was provided by Bradshaw & Wong (1972) along with some of their own data for flow over a backward-facing step (figure 1*a*). Bradshaw & Wong found a value of L (which is considered to be a typical scale of the energy-containing eddies in a plane mixing layer) equal to $0.012x$ at a downstream location $x/h = 10$ (where h is the step height and x is the downstream distance from the separation point) or about half the value in a plane mixing layer. Based on this single point measurement, they concluded that the shear layer split in half at the reattachment point and caused the sudden decrease of turbulence lengthscale. Bradshaw & Wong also argued that an alternative explanation of this drop in turbulence lengthscale at reattachment would be to suppose that the larger eddies were deflected alternately upstream and downstream rather than actually split. Measurements by both Kim, Kline & Johnston (1978) and Chandrsuda (1975) show that the intermittency is less than unity near the wall just downstream of reattachment. This result supports the alternative hypothesis of

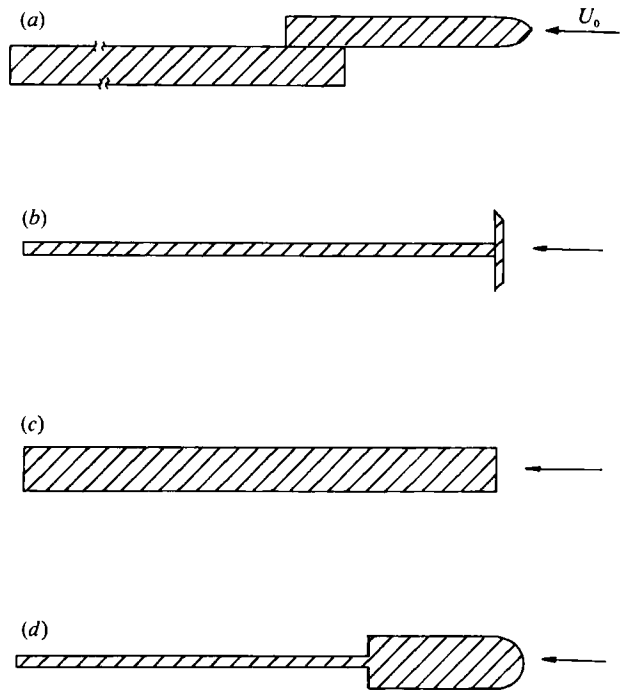

FIGURE 1. Various geometries to generate reattaching shear layer flows. (*a*) Backward facing step flow, (*b*) flow over a normal plate with splitter plate in the middle, (*c*) flow over a blunt plate, and (*d*) flow over a backward-facing step with various shapes of leading-edge nose.

Bradshaw & Wong that the eddies move alternately upstream and downstream and agree with the tentative conclusion of McGuinness (1978), who studied the large-eddy structure in a reattaching shear layer behind an orifice at the entrance of a pipe. However, a recent crude flow visualization by Eaton & Johnston (1980) showed no evidence of large eddies being swept upstream.

Other geometries with a separation and reattaching shear layer have received relatively less attention compared to backward-facing step flows. The simple case of a normal two-dimensional flat plate with a long central splitter plate in its wake (figure 1*b*) is typical of bluff body flows and has been studied recently by Ruderich & Fernholz (1986) and Castro & Haque (1987).

Ruderich & Fernholz (1986) showed self-similar behaviour for the mean and fluctuating quantities in a short region upstream of reattachment and 'profile similarity' in the separated shear layer and along the splitter plate downstream from reattachment. The data of Castro & Haque (1987) indicate that the turbulence structure of the separated shear layer differs from that of a plane mixing layer between two streams. On the other hand, several authors (Baker 1977; Kim *et al.* 1978; Eaton & Johnston 1980) have pointed out the similarity of the reattaching shear layer over a backward-facing step flow to a mixing layer.

Another geometry of a reattaching shear layer, i.e. the forward-facing blunt plate (figure 1*c*), has received some attention from, among others, Cherry, Hillier & Latour (1984) and Kiya & Sasaki (1983). A common feature of these flows is the presence of a low-frequency unsteadiness associated with a low-frequency flapping of the shear layer. While the explanation of this low-frequency unsteadiness remains inconclusive, this phenomenon has also been observed clearly in step flows (Eaton & Johnston 1980) and flows over surface-mounted fences (Castro 1981).

It is now well known that both plane mixing layers (Brown & Roshko 1974; Winant & Browand 1974) and axisymmetric mixing layers (Crow & Champagne 1971; Zaman & Hussain 1980) grow by successive pairings of spanwise vortical structures. Kibens (1980) observed that a perturbed jet underwent multiple stages of vortex pairing, by which the natural shear layer instability frequency reduced to the 'jet column' instability frequency. The 'jet column' mode of instability is more commonly known as the 'preferred mode' of a jet. The dominant structure of a mixing layer is also identified as the 'preferred mode'.

The pairing of the shear layer vortices in a backward-facing step flow has been reported previously by, among others, Rothe & Johnston (1979), Eaton & Johnston (1980) and Roos & Kegelman (1986).

In recent years, the dynamics of the coherent structures, the nature of the shear layer instability wave itself and the role of the coherent structures in mixing, heat transfer and in jet noise have been investigated extensively through experimental, theoretical and computational research for unbounded shear flows. The same is not true for bounded shear flows.

Although numerous studies of the basic flow over a backward-facing step have been conducted to date (see Eaton & Johnston 1981 for a review), only recently has attention been focused on the coherent vortical structure in a reattaching shear layer (Eaton & Johnston 1980; Pronchick & Kline 1983; Troutt, Scheelke & Norman 1984). Later, Bhattacharjee, Scheelke & Troutt (1986) and Roos & Kegelman (1986) studied the flow over a backward-facing step with a controlled perturbation. Bhattacharjee *et al.* (1986) claimed that the most effective non-dimensional forcing frequency St_h ($\equiv fh/U_0$, where f is the natural roll-up frequency of the shear layer and U_0 the free-stream velocity) was between 0.2 and 0.4. Roos & Kegelman (1986) found the natural instability frequency of the shear layer to be at $St_h = 0.4$ for laminar separation. A universal St_h value similar to the preferred mode of a jet (Hussain & Zaman 1981) or a mixing layer has yet to emerge for a reattaching shear layer.

The objectives of this paper are to study the nature of the instability wave, its roll-up into an organized large-eddy structure and the subsequent evolution of this structure in a flow over a backward-facing step under controlled perturbation. The role of controlled perturbation in modifying, and thus ultimately controlling, the flow field will also be studied.

2. Experimental apparatus and techniques

2.1. *Description of the test facility and the step*

The experiments were performed in the subsonic wind tunnel of the Mechanical Engineering Department at KFUPM. The cross-section of the test section is 1.1 m by 0.8 m, with the length being 3 m. The velocity range in the test section was 2.5 to 25 m/s, and the free-stream turbulence level was 0.1% of the free-stream velocity at 5.5 m/s.

A two-dimensional backward-facing step with an aspect ratio of 20 and step height $h = 3$ cm was used. The schematic of the test set-up is given in figure 2(*a*). All working surfaces were constructed from smooth laminated wood. The two-dimensionality of the flow was checked by measuring the longitudinal mean and fluctuation velocity at four spanwise locations at $x/h = 2$ and 13 (details of which have been given in Khan 1990). Also, a smoke wire placed along the spanwise direction at a height of 2 mm from the plate surface and 4 cm upstream of the

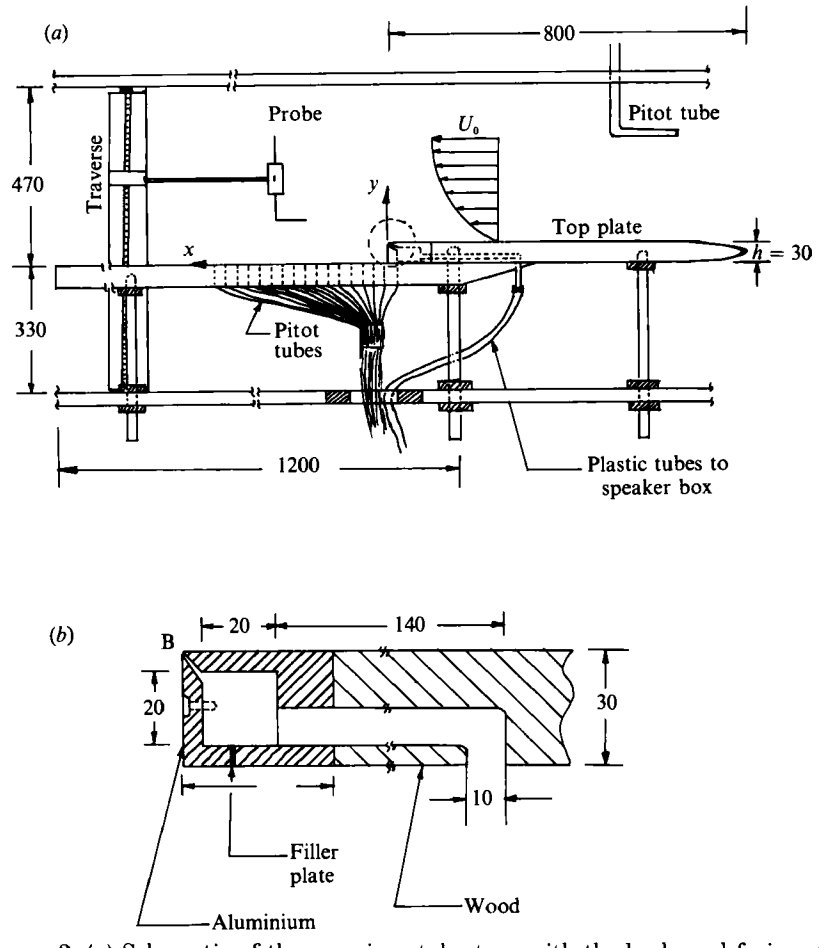

FIGURE 2. (*a*) Schematic of the experimental set-up with the backward-facing step. (*b*) Details of the perturbation system. All dimensions are in mm.

separation point showed laminar two-dimensional flow in the spanwise direction at separation. The downstream length of the bottom plate from the separation point was 100 cm. Along the centreline of the bottom plate, 2 mm diameter holes were drilled 2 cm apart to measure the surface static pressure distribution with Pitot tubes.

2.2. *The perturbation technique*

The perturbation technique used in this study was similar to those used by Hasan (1983) and Kibens (1980) to study the axisymmetric jet flow structures. The flow perturbation was introduced through a narrow slit of 1 mm width at the separation point. The details of the separation point are shown in figure 2(*b*).

The 20×20 mm cavity in the aluminium section was connected to four copper tubes of 10 mm diameter. The ends of the copper tubes were connected to the speaker box with 12 mm tygon tubes of equal length. The equal length of the tubes ensured that the perturbation at point B would be at the same phase across the whole width of the plate. The variation of perturbation amplitude was less than 5% in the spanwise direction over 4 step heights. A 30 cm diameter loudspeaker (150 W) was driven by a signal generator and an audio amplifier to introduce the perturbation at desired frequencies.

2.3. *The measurement instrumentation*

The velocity data were measured with a DISA 55 M01 standard hot-wire anemometer system. The anemometer was operated in the constant-temperature mode with a 50% overheat ratio. The hot-wire signal was linearized because of the high level of turbulence intensity present in the flow field. The probe was moved in the x- and y-directions (and for some cases in z) by a remote controlled traverse system. The resolution of the traverse system was 0.06 mm. The coordinate system for the measurements is shown in figure 2(*a*). The spectral analysis of the velocity signal was performed with a B & K 2033 high-resolution signal analyser with 400 lines. Each spectrum represents the average of 64 spectra. The hot-wire data from both the reference probe and the moving probe, as well as the signal generator output, were recorded in a 4-channel B & K 7033 tape recorder for later analysis.

Wall static pressures were measured with Pitot holes on the bottom plate. The resolution of the pressure measurement manometer was 0.01 mb.

Flow in a reattaching shear layer is complicated by the presence of recirculation, reverse flow and a high level of turbulence intensity. These factors impose some restrictions on the accuracy of conventional hot-wire measurements. A comparison of pulsed-wire and single-hot-wire measurements in a backward-facing step flow by Eaton & Johnston (1980) showed good agreement between the two measurement techniques in the region of peak turbulence intensity, i.e. near the centre of the shear layer. They established that the single-hot-wire measurements of u^2 are expected to be lower than those taken with a pulsed wire, although probably by only 1 or 2%. For flow over a normal plate, Castro & Haque (1987) and Jaroch & Fernholz (1989) showed that on $\times$-wire can undermeasure the Reynolds stresses compared to pulsed-wire measurements. It should be emphasized that most of the data presented here were measured in the outer part of the shear layer where hot-wire measurements are reliable. The reader should be cautioned that the data in figure 14 are most likely to be affected because of hot-wire usage. The peak values in figure 14 are expected to be lower than the actual values by as much as 10%, the latter being presented mainly to give a qualitative impression of the flow structure rather than for any precise quantitative interpretation.

The reattachment point was determined by a surface-oil visualization technique. The position of reattachment point usually changes. The accuracy of the surface-oil visualization technique is estimated to be $\pm 0.5h$.

Most of the measurements, unless otherwise specified, were made for a free-stream mean velocity, U_0, of 5.5 m/s, equivalent to a Reynolds number, Re_h, of 11000 based on the step height h. The corresponding Re_θ (Reynolds number based on the separation momentum thickness θ) was 240. For perturbed cases, the perturbation level, u_p/U_0, at $x = 0$ was always 1.5% at the $Y_{0.9}$ (where $U/U_\infty = 0.9$) transverse location. This was monitored continuously with a fixed reference probe. At the $Y_{0.75}$ location, the corresponding perturbation level was approximately 2.5%.

3. Results and discussion

3.1. *The initial condition*

In reattaching flows, one of the most important dependent parameters characterizing the flow field is the reattachment length, x_R, which varies between $4.9h$ and $8.2h$ for the turbulent reattaching flows with horizontal separation. Among the principal parameters affecting x_R is the initial condition of the boundary layer, i.e. the state

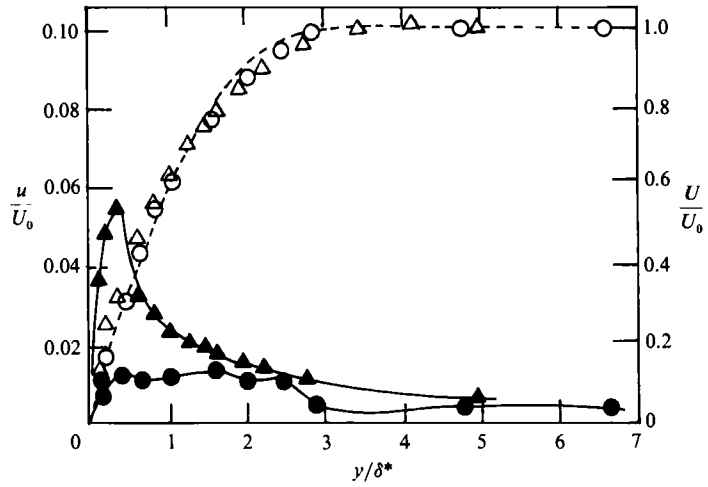

FIGURE 3. Normalized longitudinal mean velocity U/U_0 (open symbols) and fluctuation intensity u/U_0 (solid symbols) profiles of the boundary layer at the separation point for $U_0 = 5.5$ m/s: -----, the Blausius profile; ○, unperturbed flow; △, perturbed flow for $St_h = 0.314$.

f (Hz)	δ^* (mm)	θ (mm)	$H = \frac{\delta^*}{\theta}$
0	1.5519	0.6555	2.37
57.5	1.3645	0.6762	2.02

TABLE 1. Boundary-layer parameters for $U_0 = 5.5$ m/s.

of the boundary layer (laminar/turbulent) at separation. The significance of the initial condition in the reattaching shear layer was first recognized by Eaton & Johnston (1980). Thus, it is important to document the boundary-layer data at separation.

Figure 3 shows the mean velocity U and longitudinal fluctuation intensity u profiles for both natural (unperturbed) and perturbed flows at $x = 1$ mm downstream of the separation point for $U_0 = 5.5$ m/s. These data represent the initial state of the separating boundary layer. The dotted line in figure 3 is the Blasius profile and shows good agreement with the mean velocity profiles, suggesting that the separation boundary layer is laminar. The perturbed flow in figure 3 is for the $St_h = 0.314$. Note that, as a result of perturbation, the mean velocity increases slightly for $0 < y/\delta^* < 1$ (δ^* is the boundary-layer displacement thickness), while it shows a slight decrease for $2 < y/\delta^* < 4$. The perturbation increases the peak turbulence intensity level from 0.015 to nearly 0.06. This significant increase in peak turbulence intensity is due to more organized and coherent vortex shedding from separation as a result of perturbation compared to the unperturbed flow. All the data reported in this paper are for the initial conditions shown in figure 3. The boundary-layer parameters corresponding to the data in figure 3 are shown in table 1.

Among other measures, the effect of controlled perturbation on the flow field can best be described by the reattachment length, x_R, which in turn affects the surface pressure (p) distribution along the bottom plate.

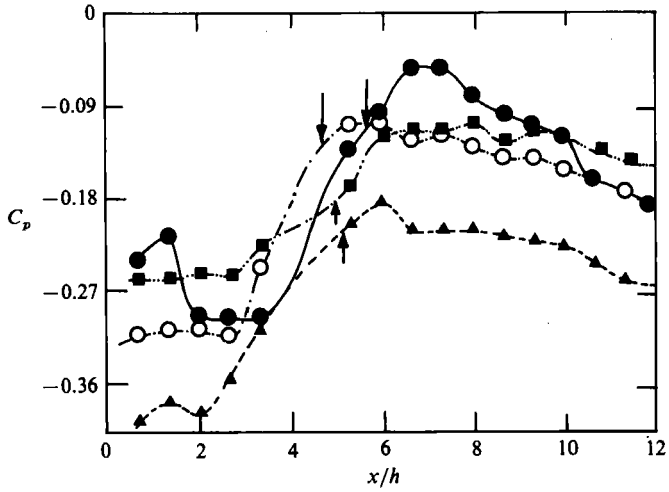

FIGURE 4. Surface static pressure coefficient C_p for unperturbed and perturbed flow for $u_0 = 5.5$ m/s. The St_h values are: ●, 0; ○, 0.218; ▲, 0.49; ■, 0.845.

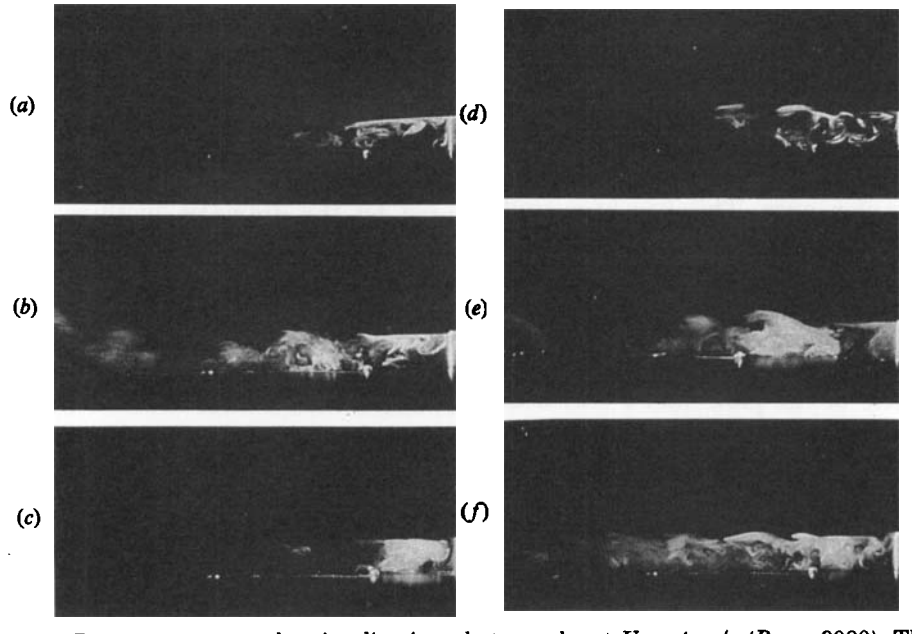

FIGURE 5. Instantaneous smoke visualization photographs at $U_0 \approx 4$ m/s ($Re_h \approx 9000$). The flow is from right to left.

3.2. *The surface pressure distribution*

The mean static surface pressure distribution in x is shown in figure 4 for both unperturbed and perturbed flows. The pressure distribution is expressed in terms of the pressure coefficient C_p, defined as

$$C_0 = (p - p_0)/0.5\rho U_0^2.$$

The arrows in figure 4 indicate the mean reattachment point obtained by surface-oil visualization. Compared to the variation of C_p for unperturbed flow, perturbation at all frequencies shifts the reattachment point approximately one step height upstream and lowers the maximum C_p value. Castro & Haque (1988) noted that the

reattachment length decreased with increasing turbulence level for flow over a normal plate with splitter. The C_p value for Castro & Haque's experiment did not change with increasing turbulence level, suggesting only an upstream shift of the entire flow field. For the present study, the change in C_p values results from the change in the organized large-scale structure due to perturbation. The basic effect of the perturbation appears to be an increased growth rate of the shear layer and thus the upstream shift of the reattachment point. A similar upstream shift of the reattachment point in backward-facing step flows due to perturbation have been reported by Bhattacharjee *et al.* (1986) and Roos & Kegelman (1986).

Roshko & Lau (1965) first proposed a modified pressure coefficient C_{pw} defined by

$$C_{pw} = (C_p - C_{\min})/(1 - C_{p\min}),$$

(where $C_{p\min}$ is the minimum value of C_p) for static pressure data of a reattaching shear layer. The wall static pressure data of figure 4 were used to calculate C_{pw}. Its peak value was the minimum (≈ 0.12) for perturbation at $St_\theta \approx 0.018$. Perturbation at $St_\theta \approx 0.017$ has been found to suppress the turbulence intensity of axisymmetric jet and plane mixing layers (Zaman & Hussain 1981) as well as axisymmetric jet noise (Hussain & Hasan 1985) via large-scale coherent structure modifications. The strong correlation between the minimum C_{pw} peak and the perturbation at $St_\theta \approx 0.018$ indicates that the peak value of C_{pw} is a reflection of the energetic large-eddy structures in the shear layer passing through the reattachment point.

3.3 *Some visual observations*

Flow visualization plays a critical role in understanding turbulent flows, especially the complex ones. This has been underscored by the dramatic pictures of large organized structures in a plane mixing layer by Brown & Roshko (1974). While flow visualization may not provide enough quantitative data, it gives significant information crucial to understanding the flow and interpreting the measurements. Keeping this in mind, some visualization experiments were performed with $U_0 \approx 4.0$ m/s. The flow was seeded continuously with smoke. The (x, y)-plane along the centre of the plate (i.e. $z = 0$) was illuminated with a laser sheet of light. The pictures were taken with a minolta SLR camera using Kodak ASA 1000 film.

A number of photographs showing various instantaneous events observed during visualization for the unperturbed flow are presented in figure 5. The flow is from right to left. The step is visible at the right-hand edge of the photographs.

Figure 5 (*a*, *b*) shows rolled up vortices after separation and merger of the vortices. In figure 5 (*b*), the merging of two vortices is very clearly observed at $x/h \approx 3.5$, where the cores of the paired vortices are still visible. These photographs confirm that the reattaching shear layer grows by vortex merging similar to plane mixing layers.

After separation, one would expect the shear layer to deflect downward and reattach on the bottom plate. The downward deflection of the shear layer seen in figure 5 (*a*) was not continuous, but it reversed intermittently. The reattachment point was found to be unsteady and moved upstream intermittently in bursts. The sudden upstream shift of the reattachment point appeared to split the shear layer into two halves (figure 5*c*), which has not been reported previously. The upstream shift of the reattachment point compressed the fluid trapped underneath the shear layer. Most of the compressed fluid was ejected by pushing the shear layer outward. The early phase of the shear layer outward movement is captured in figure 5 (*d*), which also shows the remerging of the split shear layer. The structures of the two layers are locked like chain links. Three pairs of structures are simultaneously visible,

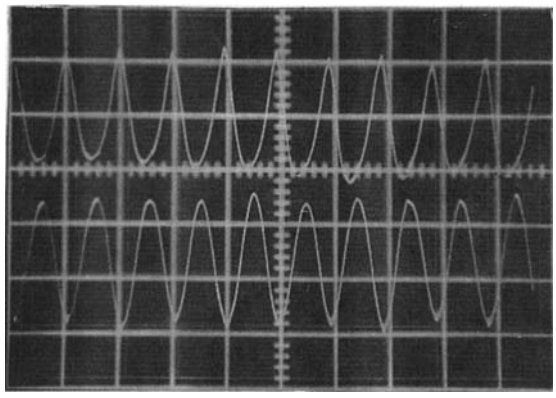

FIGURE 6. Oscilloscope trace of outer shear layer velocity signal at $x = 2$ cm and the $Y_{0.99}$ location for $f = 100$ Hz (top trace, 0.2 V/div.), and the speaker input (bottom trace, 10 mV/div). Horizontal scale: 10 ms/div.

which cannot be the regular vortex merging process observed in figure 5(*b*). The shear layer split described here is different from Bradshaw & Wong's hypothesis of splitting of the shear layer structure at the reattachment region. A later phase of the shear layer outward movement is shown in figure 5(*e*). Also, in figure 5(*e*), the structure observed close to the wall between $x/h = 2$ and 3 appeared to move towards the right, apparently split from structures travelling downstream. Figure 5(*f*) shows another phase of the flow, where one can see a highly turbulent inner layer.

The downward and upward deflections of the shear layer represent a low-frequency flapping of the shear layer, also reported by others for reattaching flow over various geometries (Eaton & Johnston 1980; Cherry *et al.* 1984; Kiya & Sasaki 1983). We believe that the low-frequency flapping of the shear layer plays a major role in the splitting of the shear layer. Whether the shear layer will split in the absence of the low-frequency flapping or with turbulent separation remains unanswered.

In order to gain further insight into the behaviour and characteristics of the large-scale structures of a reattaching shear layer, the velocity field was investigated with and without perturbation.

3.4. *The instability characteristics*

In recent years, a series of studies, both experimental (Sato 1960; Freymuth 1966; Miksad 1972; Browand 1966; Husain & Hussain 1983, among others) and theoretical (Michalke 1965; Kelly 1967) have addressed the understanding of the growth of a small-amplitude disturbance in a shear layer with laminar separation. From these studies, much has been learned about the instability, the transition from laminar to turbulence and the growth of a shear layer as well as the dynamics of the large-scale structures in unbounded shear layers, such as jets, wakes and mixing layers. In order to understand the instability characteristics of a backward-facing step flow, the flow was perturbed at the separation point at discrete frequencies.

Figure 6 is a typical oscilloscope trace showing both the velocity signal as seen by the hot-wire probe and the input signal to the speaker for perturbation frequency $f = 100$ Hz. The hot-wire signal was measured at $x = 2$ cm and the $Y_{0.99}$ location. Note that the outer layer of the flow field is highly periodic with a frequency equal to the driving frequency of the speaker. The hot-wire signal shows slight non-linearity,

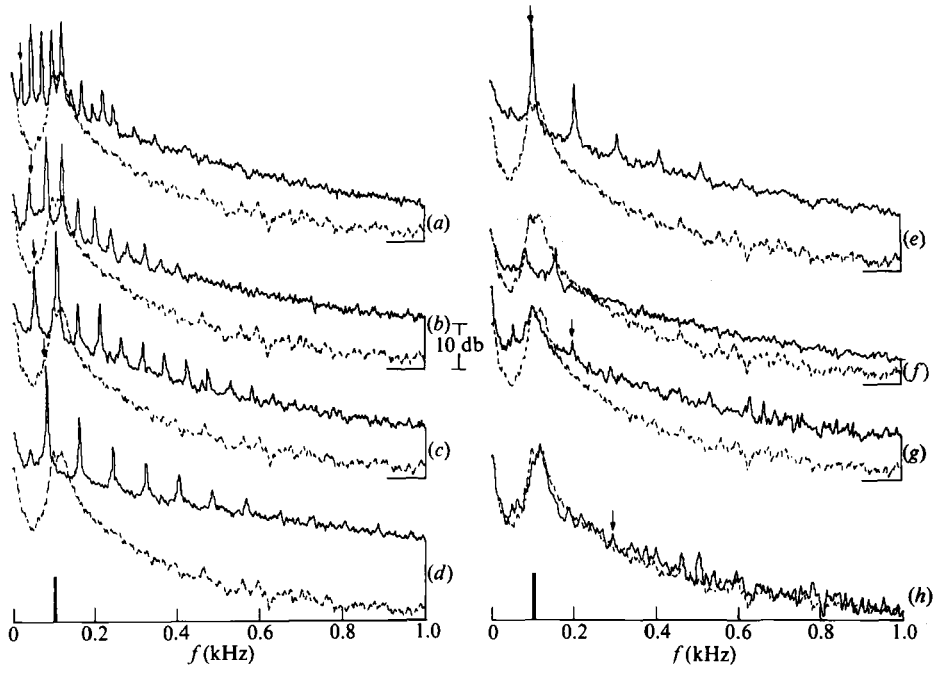

FIGURE 7. Longitudinal velocity spectra for both perturbed (solid) and unperturbed (dotted) flow at $x/h = 2$ and the $Y_{0.95}$ location. The St_h values are (*a*) 0.136; (*b*) 0.218; (*c*) 0.314; (*d*) 0.436; (*e*) 0.55; (*f*) 0.82; (*g*) 1.07; (*h*) 1.52.

instead of being purely sinusoidal. The reason for this nonlinearity is the high level of perturbation amplitude.

Effects of perturbation on the flow field are best demonstrated by the changes in longitudinal fluctuation intensity and velocity spectra.

Figure 7 shows u-spectra for different perturbation frequencies along with the unperturbed spectrum at $x/h = 2$ and the $Y_{0.95}$ location. The perturbation frequency, f, is marked with an arrow. The vertical scale in figure 7 is arbitrary, because the primary emphasis is on the frequency content and not on absolute energy levels.

3.4.1. *The natural instability frequency of the shear layer*

Note that the unperturbed spectrum (i.e. the dotted spectrum) in figure 7 shows a peak at $f \approx 100$ Hz, the corresponding St_θ and St_h values being 0.012 and 0.55 respectively. At $x/h = 2$, Roos & Kegelman (1986) observed a spectral peak at $St_h \approx 0.41$ for unperturbed flow over a backward-facing step with laminar separation. They also observed a spectral hump at $St_h \approx 0.8$, and thought this to be associated with the natural instability of the shear layer; but measurements closer to the separation point revealed no peak at $St_h \approx 0.8$. This led Roos & Kegelman (1986) to suggest that the natural instability of the reattaching shear layer was at $St_h \approx 0.40$. Bhattacharjee *et al.* (1986) found the most effective forcing frequency of a reattaching shear layer with non-laminar separation to vary between $St_h = 0.2$ and 0.4. The large disparity in the St_h values clearly indicates that the natural instability frequency for a reattaching shear layer does not scale with h. On the other hand, the natural instability (roll-up) frequency of a jet exit shear layer was found to be at $St_\theta \approx 0.012$ by Zaman & Hussain (1980). The natural shear layer instability frequency at $St_\theta \approx 0.012$ has also been confirmed for other unbounded shear flows (Sato 1960; Husain & Hussain 1983; Hussain & Hasan 1983; among others). Eaton & Johnston

(1980) observed a spectral peak at $St_h \approx 0.65$ for $x/h \leqslant 2$ for a natural flow over a backward-facing step with laminar separation. The St_h value when converted with θ represented $St_\theta \approx 0.013$. It should be pointed out that Eaton & Johnston used a step height of 5.08 cm, which was different from ours. Neither Bhattacharjee *et al.* (1986) nor Roos & Kegelman (1986) reported their θ values. This prevented us from calculating the St_θ values corresponding to their St_h values associated with the natural instability of the flow. A parallel study in our laboratory (Khan 1990) with different velocities, and thus with different θ-values, showed the natural instability frequency at $St_\theta \approx 0.012$. Thus, it is suggested that the peak in figure 7 for the unperturbed spectrum is the natural instability frequency of the reattaching shear layer and it scales with momentum thickness θ rather than with the step height h previously suggested. The spectral peak at $St_\theta \approx 0.012$ for both the free shear layer and the reattaching shear layer indicate that the instability characteristics for these two types of shear layers are similar. In figure 7, the thick vertical line on the x-axis represents $St_\theta \approx 0.012$.

3.4.2. *The effect of perturbation on u-spectra*

A comparison between the unperturbed and perturbed spectra in figure 7 shows a significant increase in the broadband turbulence level over the entire frequency band for perturbation St_h between 0.136 and 0.55 (figure 7 *a–e*). The increase in broadband turbulence level represents increased organization of the large-scale structures due to perturbation. Also, stable vortex pairing induced via perturbation can increase the overall turbulence intensity level compared to the natural flow (Zaman & Hussain 1980). Note that the subharmonic ($\frac{1}{2}f$) peaks present in figure 7 (*d* and *e*) represent pairing of the shear layer vortice, and thus contribute to the broadband increase in turbulence intensity. The pairing of the shear layer vortices has been clearly show in figure 5 (*b*).

In figure 7 (*f*), perturbation at $St_h \approx 0.82$ shows suppression of the turbulence level below the unperturbed level for $70 \leqslant f \leqslant 200$ Hz and increase of the turbulence level for $f > 200$ Hz. This can be explained by the fact that a laminar free shear layer perturbed at $St_\theta \approx 0.017$ suppressed the overall turbulence intensity (Zaman & Hussain 1981) below its unperturbed level. Zaman & Hussain (1981) did not observe any pairing event for perturbation at $St_\theta \approx 0.017$. The growth of the instability wave was maximized at $St_\theta \approx 0.017$, causing the instability wave to saturate earlier in x and thus suppress the turbulence intensity level of the flow. In figure 7 (*f*), note that the corresponding St_θ is about 0.018. Later it will be shown that the growth rate of the instability wave was the maximum for this case. But, unlike Zaman & Hussain's study, figure 7 (*f*) shows a clear $\frac{1}{2}f$ peak, indicating pairing of vortices. This perhaps is the cause of the increase in turbulence level for $f > 200$ Hz. Also present in figure 7 (*f*) is a hump at $\frac{1}{4}f$, a possible indication of a second stage of pairing.

Figure 7 (*g*) shows strong $\frac{1}{2}f$ and $\frac{1}{4}f$ components for $St_h = 1.07$. The St_θ value corresponding to the $\frac{1}{2}f$ component is nearly equal to the natural instability frequency and, thus, is stronger than the peak at f. No local suppression in turbulence intensity similar to figure 7 (*f*) is observed here. Perturbation at $St_h = 1.52$ (figure 7) shows no effect on the velocity spectrum compared to the unperturbed case.

3.4.3. *The 'step mode' of instability*

The presence of one stage of pairing in figure 7 (*d*, *e*) and two stages of pairings in figure 7 (*f*, *g*) led us to examine what limited the number of pairing stages. It appears

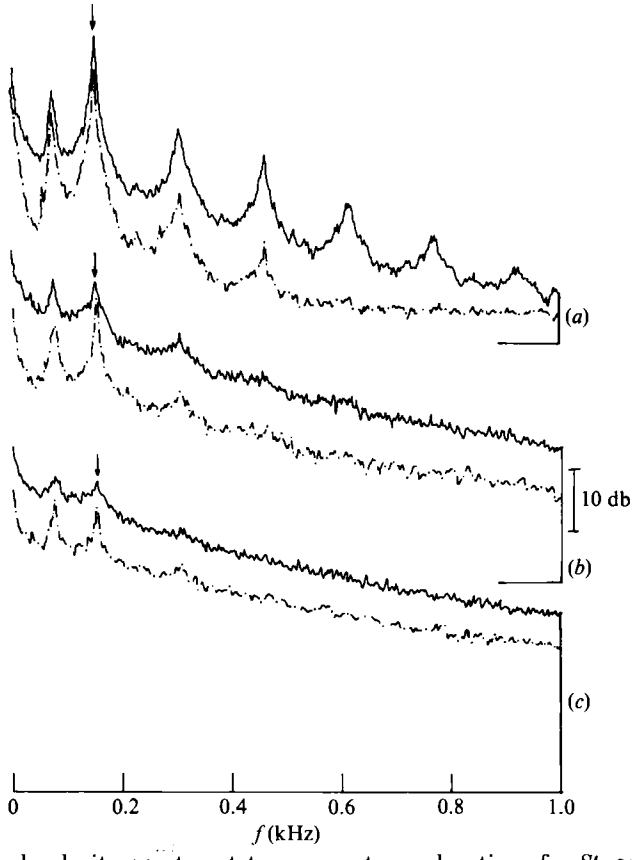

FIGURE 8. Longitudinal velocity spectra at two cross-stream locations for $St_h \approx 0.84$. Solid and dotted spectra are along $Y_{0.75}$ and $Y_{0.95}$ *lines respectively.* (*a*) $x = 2$ cm, (*b*) 4 cm, (*c*) 6 cm. The arrow indicates the perturbation frequency.

that the shear layer vortices undergo pairing until the St_h value corresponding to the lowest subharmonic peak is approximately 0.2. This strongly suggests that the reattaching shear layer vortices go through pairing until the 'shear layer' instability frequency is reduced to a final instability frequency equivalent to the 'preferred mode', discussed previously. We term this final instability frequency at $St_h \approx 0.2$ the 'step mode' of instability. This perhaps will explain why Bhattacharjee *et al.* (1986) and Roos & Kegelman (1986) observed very strong organization of the large-scale structures for perturbation at $St_h \approx 0.2$. It should be pointed out that for unperturbed flow over a backward-facing step, Eaton & Johnston (1980) observed a spectral peak at $St_h \approx 0.2$ for $x/h \approx 4$, but for $x/h \geqslant 6$ the St_h value was approximately 0.08. While an additional stage of pairing is a possibility beyond four step heights, it is our belief that the drop in St_h value around the reattachment point is due not to pairing but to the intermittent upstream sweep of the large-eddy structure at the reattachment point. In fact, Troutt *et al.* (1984) observed that the pairing interactions were strongly inhibited in the reattachment region.

3.4.4. *Transverse extent of large-eddy activities*

For a reattaching shear layer, the wall imposes a restraining effect on the downstream development of the large-eddy structures. Thus, it would be instructive to identify the range of large-eddy activity in the transverse direction.

The u-spectra for $St_h \approx 0.84$, measured along the $Y_{0.95}$ and $Y_{0.75}$ lines at three downstream locations are shown in figure 8, represented by dotted and solid lines respectively. As expected, the spectral intensity or the broadband turbulence level is higher at $Y_{0.75}$ than at $Y_{0.95}$. The first subharmonic peak ($\frac{1}{2}f$ peak) is present at both transverse locations of the shear layer for all three downstream locations, but the relative levels of both f and $\frac{1}{2}f$ components with reference to the broadband turbulence level are lower at $Y_{0.75}$ than at $Y_{0.95}$. At $x/h = 2$ (figure 8*c*), the f and $\frac{1}{2}f$ peaks are nearly lost in the background turbulence level for the $Y_{0.75}$ position. Also note that the $\frac{1}{4}f$ component is not even present in the inner shear layer ($Y_{0.75}$) spectrum, whereas it is present in the outer shear layer ($Y_{0.95}$) spectrum (figure 8*c*). The downstream evolution of subharmonic amplitudes $u_{0.5f}$ for other perturbation frequencies also showed that the $\frac{1}{2}f$ or the $\frac{1}{4}f$ peak was present further downstream in the outer shear layer spectra. Thus, it can be argued that the identity of the large-scale structure is preserved further downstream in the outer shear layer compared to the inner shear layer (i.e. close to the wall). The loss of the structure identity in the inner shear layer is attributed to the following factors, besides the increased level of turbulence there: the splitting of the shear layer and thus the structures; and the subsequent upstream sweep of a partial structure from the lower shear layer.

3.4.5. *Downstream evolution of* u_f

The growth of wave amplitudes in a shear layer is used to identify the instability characteristics of the shear layer. The downstream distribution of the instability wave amplitude u_f along the $Y_{0.75}$ line is shown in figure 9(*a*) for various perturbation frequencies. The vertical scale in figure 9 is arbitrary. Data presented in figure 9 were taken from the longitudinal velocity spectra. The horizontal scale in figure 9(*a*) shows both x/h and x/θ values.

The overall features of the instability waves (u_f) are qualitatively similar, but their details depend on frequency (figure 9*a*). The instability wave amplitude u_f shows a nearly exponential growth region immediately after separation, followed by a non-exponential growth region to a maximum value and then decay. The maximum growth of u_f is almost identical for $St_h = 0.218$, 0.436 and 0.55.

The peak for $St_h = 0.218$ at $x/\theta \approx 80$ will be maximum if the difference in perturbation amplitude at the separation point is accounted for. This is the St_h value closest to the 'step mode' and, therefore, has the most dominant peak in figure 9(*a*). The peak for $St_h = 0.436$ at $x/\theta \approx 45$ represents the first harmonic of the 'step mode', while the other significant peak for $St_h \approx 0.55$ represents the natural instability frequency because a cross-check of Strouhal numbers shows that for $St_h \approx 0.55$ the corresponding St_θ value is 0.012. Note that the growth for other instability frequencies is significantly lower than the three cases mentioned above. With increasing Strouhal number, the peak of u_f shifts upstream. The u_f for $St_h = 0.314$, which was the available perturbation frequency closest to the subharmonic of the natural instability frequency, shows two peaks, at $x/h \approx 1$ and ≈ 2 respectively, compared to one peak for other frequencies. A similar dual peak variation was observed by Zaman & Hussain (1980) for the $u_{0.5f}$ component when the jet was perturbed at frequency f. The u_f peaks were reached by 100θ downstream, the value typically observed in other shear flows.

For a hyperbolic-tangent mean velocity profile, Michalke's (1965) spatial stability theory prediction for the most unstable disturbance frequency corresponds to $St_\theta = 0.0165$. The corresponding value was found experimentally to be 0.017 by Freymuth (1966) in axisymmetric shear layers, 0.018 by Browand (1966) in plane

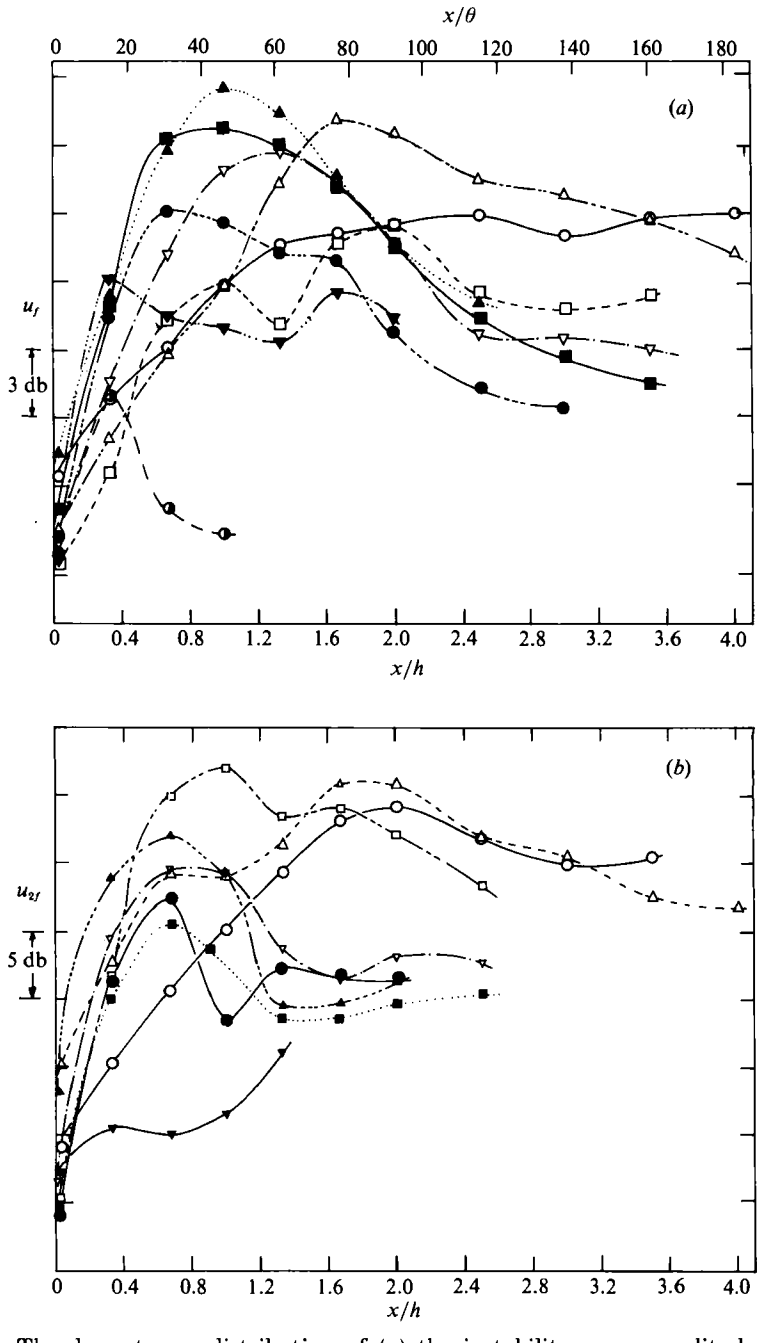

FIGURE 9. The downstream distribution of (*a*) the instability wave amplitude u_f and (*b*) the amplitude of its harmonics u_{2f}, along the $Y_{0.75}$ line. The St_h and St_θ values are ○, 0.136, 0.003; △, 0.218, 0.0048; □, 0.314, 0.007; ▽, 0.382, 0.0083; ▲, 0.436, 0.01; ■ 0.55, 0.012; ●, 0.63, 0.014, ▼, 0.85, 0.019; ◑, 0.98, 0.021.

f (Hz)	$St_h = \frac{fh}{U_0}$	$St_\theta \left(\equiv \frac{f\theta}{U_0} \right) \times 10^3$	Max. amp. (dB)	α (dB/cm)
25	0.1364	2.98	110.25	2.94
40	0.2182	4.77	114.45	4.59
57.5	0.3136	6.85	109.5	5.88
70	0.3818	8.34	112.87	7.8
80	0.4364	9.53	115.60	8.08
90	0.4909	10.70	115.70	8.25
100	0.5454	11.90	114.00	10.1
115	0.6273	13.70	110.00	12.75
135	0.7364	16.10	110.20	13.08
155	0.8455	18.50	102.00	7.67

TABLE 2. Perturbation frequencies and corresponding growth rates

water mixing layers and 0.017 by Miksad (1972) in a plane air mixing layer. However, the natural roll-up frequency of a shear layer was found to be $St_\theta \approx 0.012$, as discussed in §3.4.1. Pfizenmaier (1973) also found that the natural roll-up frequency is lower than the most unstable frequency. This suggests that for a free shear layer, the natural roll-up (instability) frequency is lower than the most unstable frequency. In order to find out if such is the case for the reattaching shear layer, the growth rate, α, for various u_f was calculated. The growth rate for each Strouhal number was obtained by drawing a tangent to the u_f curves (figure 9*a*) at $x/h = 0$ and is shown in table 2. The uncertainty in α measurement is estimated to be ± 0.65 dB/cm. Although the initial growth region for the data in figure 9(*a*) was not strictly linear like that of Freymuth (1966) and Miksad (1972), the α values show excellent qualitative agreement with those of Miksad's data. Note that the most-unstable mode frequency corresponds to $St_\theta \approx 0.017$, which is the same as that reported by others. This further strengthens our argument that a reattaching shear layer (or at least a backward-facing step flow) is very similar to that of a plane mixing layer or an axisymmetric mixing layer with respect to its instability behaviour and downstream growth.

3.4.6. *Downstream evolution of u_{2f}*

The downstream evolution of u_{2f} (the amplitude of first higher harmonic component) corresponding to the data in figure 9(*a*) is shown in figure 9(*b*). The u_{2f} component for $St_h = 0.136$ grows almost exponentially and reaches a peak value at $x/h \approx 2$. The maximum growth of u_{2f} takes place for $St_h = 0.314$ with a peak at $x/h \approx 1$. The St_θ corresponding to the $2f$ component is equal to 0.013, which is the closest to the natural instability frequency of the shear layer and, thus, would explain the maximum growth.

The non-exponential growth of the present u_f data is due to the nonlinear effect present. Since, in our study, the perturbation level was not restricted to a level below which the instability wave grows exponentially, it will be worthwhile to compare the growth of the disturbance with theoretical studies dealing with nonlinear instability waves.

3.4.7. *Comparison with theoretical predictions*

The theory for the linear spatial or temporal evolution of an instability wave in a free shear layer is now well established (Michalke 1965; Kelly 1967; Mattingly &

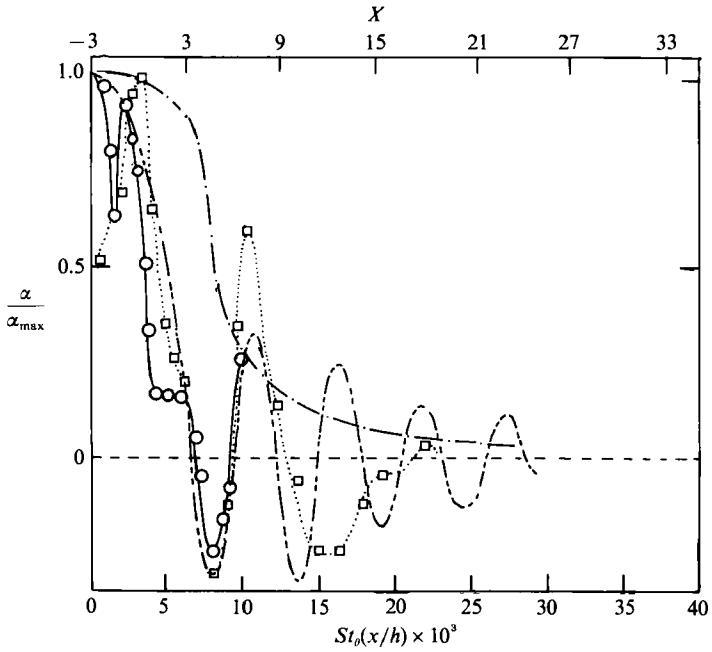

FIGURE 10. Normalized growth rate α/α_{max} (α_{max} is the growth rate at $x = 0$ cm) for u_f values of figure 9(*a*). The St_h values are: ○, 0.136; □, 0.314. —.—.—, $\Lambda = 100$ ————————, $\Lambda = 0$ (from Goldstein & Hultgren 1988).

Criminale 1972) and has been successfully compared with experimental studies. However, the theoretical treatment of the nonlinear spatial evolution of an instability wave in a free shear layer is only just beginning. In a recent work, Goldstein & Hultgren (1988) studied the nonlinear spatial evolution of an externally excited instability wave in a free shear layer. Although the present study was performed for a backward-facing step flow, we felt that Goldstein & Hultgren's results were the most appropriate for comparing to our data.

Figure 10 shows the data for two cases from figure 9(*a*) in α/α_{max} versus $St_\theta\, x/h$ coordinates, where α is the local growth rate of the instability wave, and α_{max} is the maximum of α. For our data α_{max} is the slope of u_f at $x = 0$, but for Goldstein & Hultgren's data it represents the growth rate for a linear instability wave. Note that in figure 10 the top axis is shown in X, defined by Goldstein & Hultgren (1988). Scaled growth rates of the fundamental instability wave as a function of X for two limiting values of the normalized viscous parameter Λ ($\equiv 8/[Re_\theta \Delta St_\theta]$, where ΔSt_θ is the difference between the local Strouhal number and the Strouhal number predicted by linear inviscid parallel flow stability theory) are also given in figure 10. $\Lambda = 0$ represents the inviscid case. The data show excellent qualitative, and for some cases even quantitative, agreement with theoretical predictions. It is possible that this agreement is circumstantial and will need further support to our claim that the shear layer instability of a reattaching shear layer is similar to that of a plane mixing layer.

In figure 10, note that the scaled growth rate for our data goes through an oscillation for $-3 \leqslant X \leqslant 3$, before becoming negative for $X > 3$ (the corresponding x/x_R value varies between 0.1 and 0.2). No such oscillation of the growth rate before becoming negative is observed for the theoretical curves. The oscillation or an increase of the growth rate prior to becoming negative is possibly an indirection of the shear layer splitting as it travels downstream. The splitting of the shear layer will

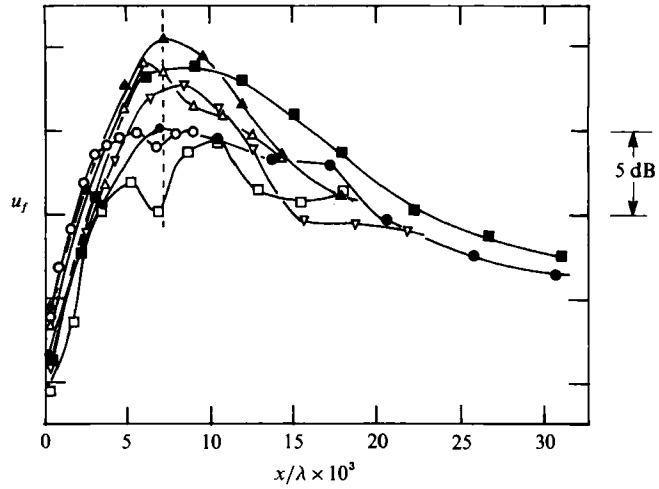

FIGURE 11. The data from figure 9(*a*) in the x/λ coordinate. The St_h values are: ○ 0.136; △, 0.218; □, 0.314; ▽, 0.382; ▲, 0.436; ■, 0.55; ●, 0.63.

change the instantaneous mean velocity (without altering the time-average mean velocity) profile and, thus, will affect the growth rate of the instability wave. In fact, the increase of the growth rate after an initial decay is possible if a secondary instability is created. It is possible that the shear layer splitting generates a new instability wave prior to the split. This is a highly speculative conclusion at best and more work will be necessary to establish the exact cause of the growth rate oscillation.

3.4.8. *Scaling of u_f growth with λ*

In figure 9(*a*) it was observed that, with increasing f, the peak amplitude of he perturbation wave moved upstream. This suggests the dependence of the instability wave growth on the acoustic wavelength, λ, (as well as on the hydrodynamic wavelength, provided the convection velocity of the wave is assumed constant) rather than on the step height h. A few cases of the data from figure 9(*a*) are plotted in figure 11 with the downstream distance x normalized by λ. Note that the peak amplitude for all perturbed frequencies occurs at $x/\lambda \approx 0.0075$. The strong dependence of the instability wave on the acoustic wavelength has not been reported previously either for an axisymmetric shear layer or for a plane mixing layer.

While the data presented in this section provide, for the first time, information on the nonlinear spatial evolution of an externally perturbed instability wave in a reattaching shear layer, they shed very little light on the effects of perturbation on the overall flow field. In order to address this question, the details of the flow field were documented with and without perturbation.

3.5. *The effects of perturbation on overall turbulence intensity*

3.5.1. *Variation of u/U_∞ with Strouhal number*

The overall level of turbulence intensity in a shear flow is generally recognized as a measure of the strength, organization and coherence of the large-eddy structures present in the flow. Figure 12(*a*) shows the normalized longitudinal turbulence intensity u/U_∞ at $x/h = 1$ and at the cross-stream location $Y_{0.99}$ for various perturbation frequencies. The dashed line shows the turbulence level for unperturbed flow. Note that the turbulence intensity level increases dramatically owing to the

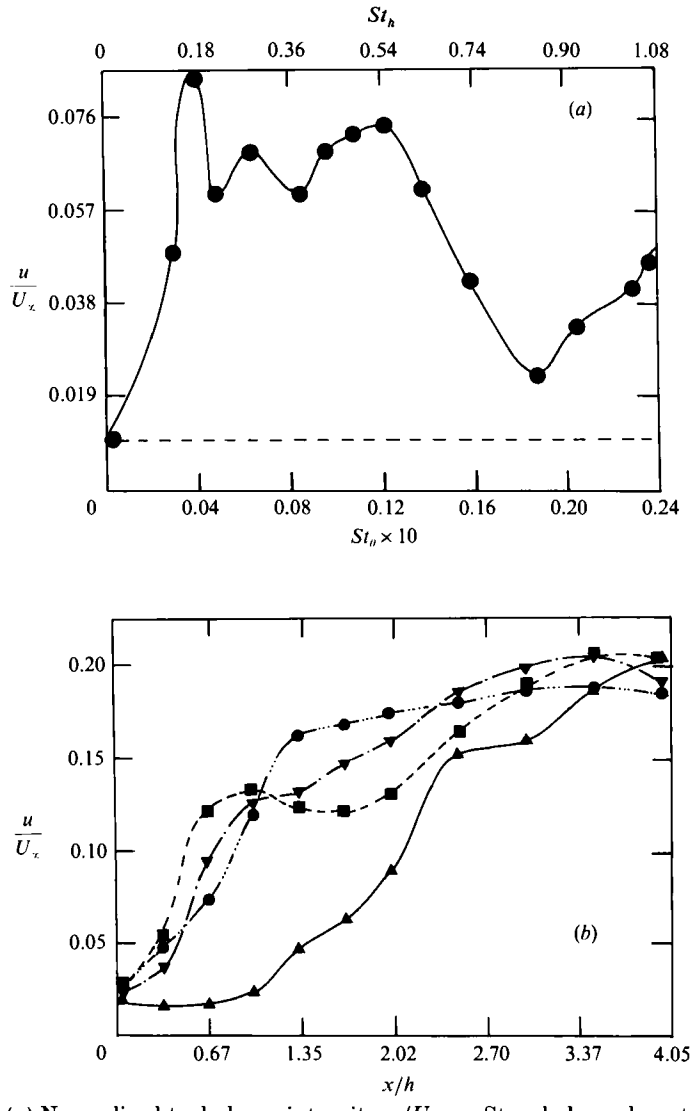

FIGURE 12. (*a*) Normalized turbulence intensity u/U_∞ *vs.* Strouhal number at $x/h = 1$ and the $Y_{0.99}$ location (i.e. $U/U_\infty = 0.99$). (*b*) The downstream variation of u/U_∞ along the $Y_{0.75}$ line. The St_h and St_θ values are: ▲, 0, 0; ▼, 0.313, 0.007; ■, 0.55, 0.012; ●, 0.736, 0.016.

perturbation and the increase is present for the whole Strouhal number range investigated ($St_h = 0.09$–1.08), which was limited by the operating range of the speaker. Between $St_h \approx 0.1$ and 0.8, the u/U_∞ data show three peaks. The first peak at $St_h \approx 0.18$ is the maximum and reinforces our claim that the most energetic structure of the step flow is at $St_h \approx 0.2$, defined as the 'step mode' of instability in a previous section, and is equivalent to the 'preferred mode' of free shear layers. The third peak is due to the instability associated with the natural roll-up frequency while the second peak is due to perturbation at the subharmonic frequency of the natural instability frequency. Similar enhancement of flow structures in plane mixing layer for subharmonic forcing was observed by Ho & Huang (1981). The 'step mode' of instability at $St_h \approx 0.18$ was independently verified in a parallel study dealing with non-laminar boundary layer at separation (Khan 1990). Similar to the

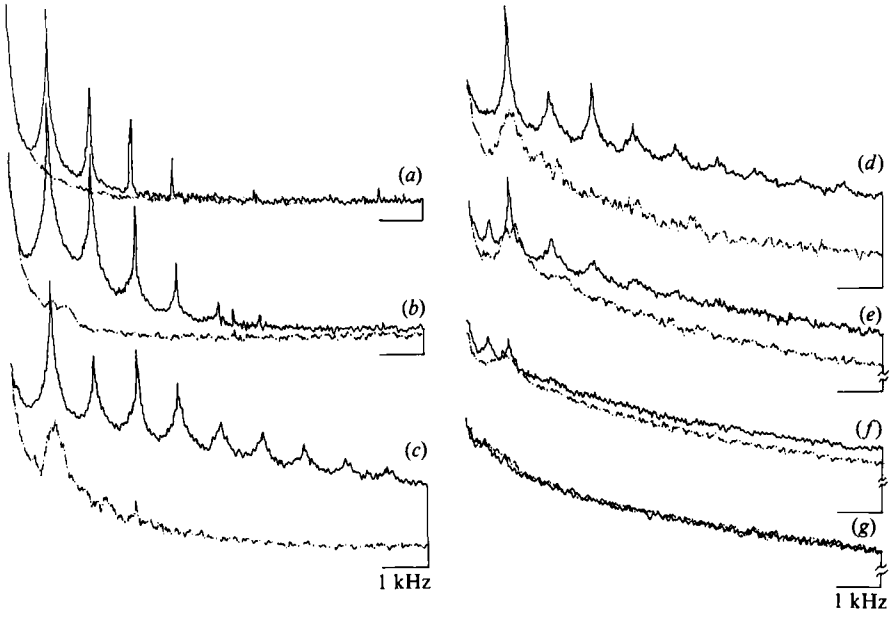

FIGURE 13. Downstream evolution of both unperturbed ($St_\theta = 0$) and perturbed ($St_\theta = 0.012$) velocity spectra along the $Y_{0.75}$ line. The downstream locations x/h are: (*a*) 0; (*b*) 0.333; (*c*) 1.0, (*d*) 1.333, (*e*) 2.0, (*f*) 3.0, (*g*) 4.0.

'preferred mode' of free shear layers, it is our opinion that the 'step mode' of instability for a reattaching shear layer is independent of the initial condition at separation. This is supported by the observation made in the other studies of perturbed flow over backward-facing steps (Bhattacharjee *et al.* 1986; Roos & Kegelman 1986). Also, note that u/U_∞ in figure 12(*a*) reaches a minimum at $St_\theta \approx 0.017$. However, the minimum u/U_∞ at $St_\theta \approx 0.017$ is higher than the turbulence level for unperturbed flow. Neither Zaman & Hussasin (1981) nor Hasan (1983) found any vortex pairing for perturbation of free shear layers at $St_\theta \approx 0.017$. But in the present study strong vortex pairing was observed for $St_\theta \approx 0.017$ (as discussed in §3.4.2). It is argued here that the maximum growth rate of the instability wave at $St_\theta \approx 0.017$ helped reduce the turbulence intensity level of the flow, while the vortex pairing increased the turbulence level – resulting in a net turbulence intensity level higher than the unperturbed level.

3.5.2. *Downstream evolution of* u/U_∞

The downstream evolution of the normalized longitudinal turbulence intensity u/U_∞ along the $Y_{0.75}$ line for a few perturbed cases is shown in figure 12(*b*). The data for unperturbed flow are also included in the figure. Note that u for all perturbed cases is higher than the corresponding unperturbed case between $x/h = 0$ and 3.5. The peak turbulence intensity occurs at $x/h \approx 4$ for the unperturbed flow while for perturbed flow the peak shifts upstream by almost one step height. This is consistent with the upstream shift, due to perturbation, of the reattachment point, discussed previously. For $St_\theta \approx 0.012$, turbulence intensity data develop an earlier peak at $x/h \approx 1$, the amplitude of this peak being always lower than the peak at $x/h \approx 4$. The peak at $x/h \approx 1$ is due to the vortex pairing present for this case. It is clear from figure 12(*b*) that the effect of perturbation on u is present up to a downstream distance of approximately four step heights.

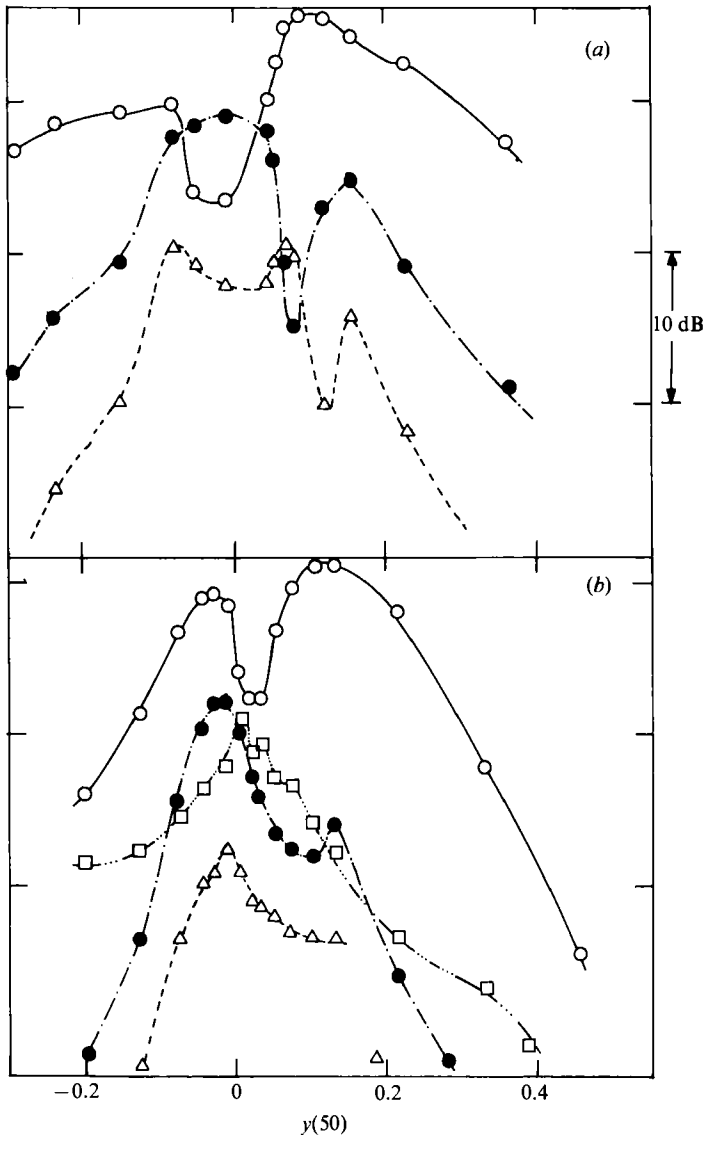

FIGURE 14. For caption see facing page.

3.5.3. *Downstream evolution of u-spectra*

Figure 13 compares the downstream evolution of the perturbed u-spectrum with its unperturbed counterpart. The flow was perturbed at $St_\theta \approx 0.012$. The spectra were measured at the transverse location $Y_{0.75}$. Note that the perturbation increases the broadband turbulence level and the amplification is maximum at $x/h = 1$. The peak at the perturbation frequency is almost lost in the background turbulence level at $x/h = 4$, and the perturbed and unperturbed spectra are identical. This is consistent with the data of figure 12 (b). For $x/h > 4$, our effort to detect the persistence of clear velocity spectral peaks failed, even for measurements in the outer shear layer. A later study (Khan 1990) found that the spectral peak at the perturbation frequency persisted as far as $x/h = 11$ for the turbulent separation boundary layer. This suggests that under perturbation, the large-scale organization is stronger for

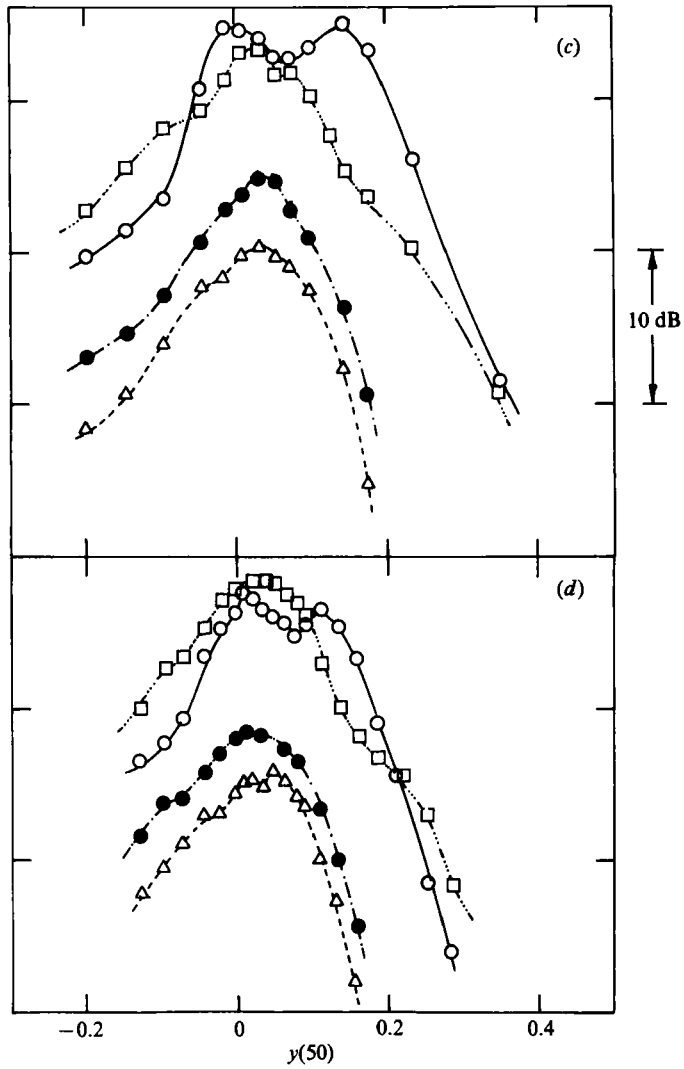

FIGURE 14. Cross-stream distribution of longitudinal spectral energy for $St_\theta = 0.012$ and its harmonics. (*a*) $x/h = 1$, (*b*) 2, (*c*) 3, (*d*) 4. The symbols are: ○, u_f; ●, u_{2f}; △, u_{3f} and □, $u_{0.5f}$.

turbulent separation compared to laminar separation. The flow visualization pictures of Roos & Kegelman (1986), with laminar and turbulent separations support this.

3.6. *Cross-stream energy distribution of large-eddy structures*

The turbulent energy distribution across the shear layer for perturbation frequency f and its harmonics at various downstream locations can be used to characterize the large-eddy structures present in the flow. Figure 14(*a–d*) shows the one-dimensional spectral energy at f and its higher harmonic components, $2f$ and $3f$, as well as the sub-harmonic component, $0.5f$ (if present), at downstream locations $x/h = 1$ to 4. Only the data for perturbation at $St_\theta = 0.012$ are shown.

Note that at $x/h = 1$ (figure 14*a*), the distribution of u_f and u_{2f} is reminiscent of the behaviour found in the wake of a cylinder (i.e. the frequency component f associated with the vortex shedding from opposite edges of the cylinder shows two peaks along the edges of the cylinder, and the $2f$ component shows a single peak along

the centreline of the cylinder). This supports our observation in figure 5(*c*) that the shear layer and, thus, the large-eddy structure splits at $x/h \approx 1$. The amplitudes of the two peaks in figure 14(*a*) are not the same. As the shear layer splits, the structure in the lower half of the shear layer appears to be weaker than the structure in the upper shear layer, a fact also supported by the spectra in figure 8. At this location, the centreline of the shear layer is at $y(50) \approx 0$, ($y(50) \equiv (y - y_{0.50})/x$) i.e. the location at which u_f and u_{2f} reach their minimum and maximum values respectively. Note that at $y(50) \approx 0.16$, both u_{2f} and u_{3f} show a second peak. A slow oscillation of the outer shear layer structure may be responsible for these second peaks.

At $x/h = 2$ (figure 14*b*), the dual peaks and the dip for the u_f component have shifted slightly away from the wall with respect to figure 14(*a*). A sub-harmonic component ($0.5f$) is present in the velocity spectrum at $x/h = 2$. The peak value of $u_{0.5f}$ is about 10 dB lower than the peak value for u_f. This sub-harmonic component is an indication of impending pairing activity in the shear layer. Note that the $u_{0.5f}$ component persists over a wider range of y in the high-velocity edge ($y(50) > 0$) than in the low-velocity edge ($y(50) < 0$) of the shear layer.

As the flow moves further downstream, at $x/h = 3$ (figure 14c), the maximum values of $u_{0.5f}$ and u_f are almost the same. A continuing pairing of two vortices usually will give similar strengths for both the u_f and $u_{0.5f}$ components, while a higher amplitude of $u_{0.5f}$ than u_f is possible after the completion of pairing. This conforms with the higher peak amplitude of $u_{0.5f}$ than u_f at $x/h = 4$ (figure 14*d*). This essentially implies that the pairing event in the shear layer is complete by $x/h = 4$, also supported by the photograph in figure 5(*b*). It should be pointed out that in figure 14(*c*, *d*), the u_{2f} and u_{3f} components disappear for $y(50)$ greater than 0.2, while u_f and $u_{0.5f}$ components are present for $y(50) \approx 0.3$. This will result if, after splitting, the influence of the lower shear layer on the upper shear layer diminishes, i.e. the lower shear layer moves away from the upper shear layer or the two shear layers remerge. More work on the energy exchange as well as the phase relationship between dominant frequency peaks across the shear layer at various downstream locations will be needed for a complete understanding of the reattaching shear layer splitting. Such a study is beyond the scope of this work. Also note that at $x/h = 4$ (figure 14*d*), the u_f and its harmonics disappear for $y(50) < -0.1$. This is because the structures are accompanied by increasing phase jitter and start breaking down around this location, giving high turbulence intensity in the region preceeding reattachment.

4. Conclusions

The flow structure and the nature of the instability wave in a reattaching shear layer, as well as the effects of controlled perturbation on such flow, have been studied experimentally for a backward-facing step geometry with laminar separation.

The reattaching shear layer showed two distinct modes of instability, i.e. the 'shear layer mode' of instability, scaling with momentum thickness θ at separation; and the 'step mode' of instability, scaling with step height h. The corresponding Strouhal numbers, St_θ and St_h, were 0.012 and 0.18. The shear layer mode of instability reduced to the step mode via one or more stages of pairing. The growth of the instability wave in the reattaching shear layer showed excellent agreement with the theoretical analyses predicting nonlinear spatial evolution of an externally perturbed instability wave in a free shear layer.

Perturbation at discrete frequencies shifted the reattachment point upstream and increased the turbulence intensity across the entire shear layer for $x/h \leqslant 4$. The

upstream shift of the reattachment point with perturbation was primarily due to the increased growth rate of the shear layer prior to reattachment.

Measurements of longitudinal fluctuating energy of the dominant structure and its harmonics across the shear layer at various downstream locations for perturbed flow strongly indicated splitting of the shear layer as it travelled downstream. Flow visualization experiments appeared to confirm that the shear layer did split into two and showed the existence of a low-frequency flapping of the shear layer. Whilst the splitting of the shear layer and its dependence on the low-frequency flapping of the shear layer are believed to be amongst the first to be reported, more definitive conclusions regarding the phase of the low-frequency flapping at which the shear layer splits must await the availability of detailed correlations and conditional sampling type of measurements.

The author would like to thank the College of Graduate Research at KFUPM for supporting the research. Thanks are due to Mr Khaled Al-Ohali and to Mr A. S. Khan for their help at various phases of this work. The author would also like to acknowledge Professor J. K. Eaton of Stanford University and the anonymous referees for bringing two related references to the author's attention, which have been cited herein, and also for the constructive criticisms of the manuscript.

REFERENCES

Baker, S. 1977 Regions of recirculating flow associated with two-dimensional steps. Ph.D. thesis, Dept. of Civil Engng, University of Surrey.

Bhattacharjee, S., Scheelke, B. & Troutt, T. R. 1986 Modification of vortex interactions in a reattaching separated flow. *AIAA J.* **24**, 623.

Bradshaw, P. & Wong, F. Y. F. 1972 The reattachment and relaxation of a turbulent shear layer. *J. Fluid Mech.* **52**, 113.

Browand, F. K. 1966 An experimental investigation of the instability of an incompressible separated shear layer. *J. Fluid Mech.* **26**, 281.

Brown, G. & Roshko, A. 1974 On density effects and large structure in a turbulent mixing layer. *J. Fluid Mech.* **64**, 775.

Castro, I. P. 1981 Measurements in shear layers separating from surface mounted obstacles. *J. Wind Engng Indust. Aero.* **7**, 253.

Castro, I. P. & Haque, A. 1987 The structure of a turbulent shear layer bounding a separation region. *J. Fluid Mech.* **179**, 439

Castro, I. P. & Haque, A. 1988 The structure of a turbulent shear layer bounding a separation region. Part 2. Effects of free-stream turbulence. *J. Fluid Mech.* **192**, 577.

Chandrsuda, C. 1975 A reattaching turbulent shear layer in incompressible flow. Ph.D. thesis, Dept. of Aeronautics, Imperial College of Science & Technology.

Cherry, N. J., Hillier, R. & Latour, M. E. M. P. 1984 Unsteady measurements in a separated and reattaching flow. *J. Fluid Mech.* **144**, 13.

Crow, S. C. & Champagne, F. H. 1971 Orderly structure in jet turbulence. *J. Fluid Mech.* **48**, 547.

Eaton, J. K. & Johnston, J. P. 1980 Turbulent flow reattachment: An experimental study of the flow and structure behind a backward-facing step. *Rep.* MD-39. Dept. of Mech. Engn., Stanford University.

Eaton, J. K. & Johnston, J. P. 1981 A review of research on subsonic turbulent flow reattachment. *AIAA J.* **19**, 1093.

Freymuth, P. 1966 On transition in a separated laminar boundary layer. *J. Fluid Mech.* **25**, 683.

Goldstein, M. E. & Hultgren, L. S. 1988 Nonlinear spatial evolution of an externally excited instability wave in a free shear layer. *J. Fluid Mech.* **197**, 295.

Hasan, M. A. Z. 1983 The effects of external and self excitations on axisymmetric jet turbulence and noise. Ph.D. thesis, University of Houston.

Ho, C. M. & Huang, L. S. 1982 Subharmonic and vortex merging in mixing layers. *J. Fluid Mech.* **119**, 443.

Husain, Z. D. & Hussain, A. K. M. F. 1983 Natural instability of free shear layers. *AIAA J.* **21**, 1512.

Hussain, A. K. M. F. & Hasan, M. A. Z. 1983 The whistler nozzle phenomenon. *J. Fluid Mech.* **134**, 431.

Hussain, A. K. M. F. & Hasan, M. A. Z. 1985 Turbulence suppression in free turbulent shear flow under controlled excitation. Part 2. Jet-noise reduction. *J. Fluid Mech.* **150**, 159.

Hussain, A. K. M. F. & Zaman, K. B. M. Q. 1981 The preferred mode of the axisymmetric jet. *J. Fluid Mech.* **110**, 39.

Jaroch, M. P. & Fernholz, H. H. 1989 The three-dimensional character of a nominally two-dimensional separated turbulent shear flow. *J. Fluid Mech.* **205**, 523.

Kelly, R. E. 1967 On the stability of an inviscid shear layer which is periodic in space and time. *J. Fluid Mech.* **27**, 657.

Khan, A. S. 1990 An experimental study of reattaching flow over a backward facing step with controlled perturbation. MS thesis, Mech. Engng. Dept., KFUPM, Dhahran, Saudi Arabia.

Kibens, V. 1980 Discrete noise spectrum generated by an acoustically excited jet. *AIAA J.* **18**, 434.

Kim, J., Kline, S. J. & Johnston, J. P. 1978 Investigation of separation and reattachment of a turbulent shear layer: Flow over a backward-facing step. *Rep.* MD-37. Thermoscience Div., Dept. of Mech. Engng, Stanford University.

Kiya, M. & Sasaki, K. 1983 Structure of a turbulent separation bubble. *J. Fluid Mech.* **137**, 83.

Mattingly, G. E. & Criminale, W. O. 1972 The stability of an incompressible two-dimensional wake. *J. Fluid Mech.* **51**, 233.

McGuinness, M. 1978 Flow with separation bubble – steady and unsteady aspects. Ph.D. dissertation, Cambridge University.

Michalke, A. 1965 On spatially growing disturbances in an inviscid shear layer. *J. Fluid Mech.* **22**, 371.

Miksad, R. W. 1972 Experiments on the nonlinear stages of free-shear-layer transition. *J. Fluid Mech.* **56**, 695.

Pfizenmaier E. 1973 On the instability of a sound influenced free jet. *Inst. für Turbulenzforsch*, Berlin.

Pronchick, S. W. & Kline, S. J. 1983 An experimental investigation of the structure of a turbulent reattaching flow behind a backward facing step *Rep.* MD–42. Thermosciences Division, Dept. of Mech. Engng. Stanford University.

Roos, F. W. & Kegelman, J. T. 1986 Control of coherent structures in reattaching laminar and turbulent shear layers. *AIAA J.* **24**, 1956.

Roshko, A. & Lau, J. C. 1965 Some observations on transition and reattachment of a free shear layer in incompressible flow. In *Proc. 1965 Heat Transfer and Fluid Mech. Inst.; Stanford University.*

Rothe, P. H. & Johnston, J. P. 1979 Free-shear-layer behaviour in rotating systems. *Trans. Asme* I: *J. Fluids Engng*, **101**, 117.

Ruderich, R. & Fernholz, H. H. 1986 An experimental investigation of a turbulent shear flow with separation, reverse flow, and reattachment. *J. Fluid Mech.* **163**, 283.

Sato, H. 1960 The stability and transition of a two-dimensional jet. *J. Fluid Mech.* **7**, 53.

Troutt, T. R., Scheelke, B. & Norman, T. R. 1984 Organized structure in a reattaching separated flow field. *J. Fluid Mech.* **143**, 413.

Winant, C. D. & Browand, F. K. 1974 Vortex pairing: the mechanism of turbulent mixing-layer growth at moderate Reynolds number. *J. Fluid Mech.* **63**, 237.

Zaman, K. B. M. Q. & Hussain, A. K. M. F. 1980 Vortex pairing on a circular jet under controlled excitation. Part 1. General jet response. *J. Fluid Mech.* **101**, 449.

Zaman, K. B. M. Q. & Hussain, A. K. M. F. 1981 Turbulence suppression in free turbulent shear flow under controlled excitation. *J. Mech.* **103**, 133.